Three-Dimensional Wideband Beamforming for Imaging Through a Single Wall

Fauzia Ahmad, *Senior Member, IEEE*, Yimin Zhang, *Senior Member, IEEE*, and Moeness G. Amin, *Fellow, IEEE*

***Abstract*—Through-the-wall imaging and urban sensing is an emerging area of research and development. The incorporation of the effects of signal propagation through wall material in producing an indoor image is important for reliable through-the-wall mission operations. We have previously analyzed wall effects, such as refraction and change in propagation speed, and designed a wideband beamformer for 2-D imaging using line arrays. In this letter, we extend the analysis to 3-D imaging via delay-and-sum beamforming in the presence of a single uniform wall. The third dimension provides valuable information on target heights that can be used for enhancing target discrimination/identification. Supporting simulation results are provided.**

***Index Terms*—Beamforming, radar imaging, through-the-wall, urban sensing.**

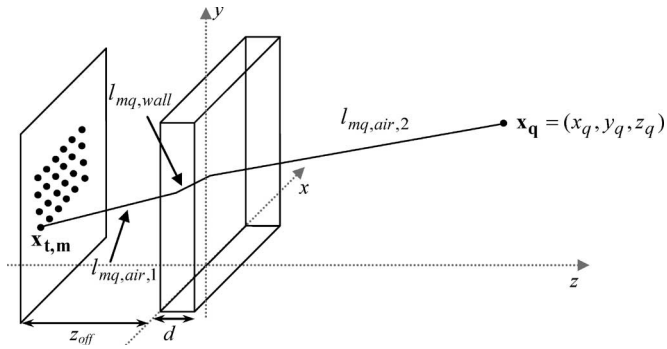

Fig. 1. Geometry on transmit for 3-D imaging.

I. Introduction

URBAN rescue and offensive operations face challenges due to difficulty in target detection and identification in enclosed structures and behind walls. The ability to sense and see through walls can be advantageous to resolve conflicts in urban environments. A through-the-wall imaging (TWI) and sensing system can provide enhanced situational awareness for urban operations [1]–[4]. In particular, a TWI system should facilitate real-time target detection, target localization with high range and crossrange resolutions, and target classification and identification.

In [4] and [5], we presented a wideband near-field delay-and-sum beamformer for 2-D TWI using line arrays. The effects of signal propagation through dielectric walls, such as refraction and change in propagation speed, were incorporated into the design for accurate and reliable target localizations. Techniques were also devised for mitigating the detrimental effects of unknown walls on imaging quality and reliability [5], [6].

In this letter, we extend our work in [4] and [5] to 3-D imaging using planar arrays. In addition to range, 3-D imaging of scenes behind walls provides valuable information about the target extent in length, height, and width. This additional feature is instrumental to effective target classification/identification. We consider the case where the transmitters and the receivers are looking through a single known uniform wall. It is noted that, once the approach for 3-D imaging is established for known walls, the techniques introduced to handle 2-D imaging in the presence of unknown walls can be applied directly, without any modification, to the 3-D imaging problem.

II. Three-Dimensional Through-the-Wall Beamforming

Consider an M-element transmit planar array, located at $\{\mathbf{x_{tm}} = (x_{tm}, y_{tm}, -z_{\text{off}}\}_{m=1}^{M}$, and a planar array of N receivers, located at $\{\mathbf{x_{rn}} = (x_{rn}, y_{rn}, -z_{\text{off}}\}_{n=1}^{N}$. The parameter z_{off} represents the standoff distance of the arrays from a uniform wall of thickness d and dielectric constant ε, located in the $x-y$-plane, as shown in Fig. 1. The region to be imaged is located beyond the wall along the positive z-axis. Let $s(t)$ denote the wideband signal used for interrogating the scene. The scene is divided into voxels in downrange, crossrange, and height, represented by the z, x, and y coordinates, respectively. An image is generated using the delay-and-sum wideband beamforming technique, which involves forming focused transmit and receive beams and sweeping the beams electronically across all voxels in the region of interest [7]. That is, the pulse $s(t)$ is emitted from each transmitter with relative time delay so that all transmitted pulses simultaneously reach a particular location, for example, the qth voxel located at $\mathbf{x_q} = (x_q, y_q, z_q)$. Likewise, on reception, beamforming amounts to applying delays to the outputs of the N receivers so as to synchronize the signal arrivals from $\mathbf{x_q}$ across all receivers and then summing the delayed signals. These focusing delays, applied on transmission and reception, are adjusted to sweep the beams across all voxels in the image. Additional weights can be applied to control the shape and sidelobe structure of the

Manuscript received May 23, 2007; revised September 12, 2007. This work was supported by the Defense Advanced Research Projects Agency under Contracts HR0011-06-C-0110 and HR0011-07-1-0001. The content of the information does not necessarily reflect the position or the policy of the U.S. Government, and no official endorsement should be inferred.

The authors are with the Radar Imaging Laboratory, Center for Advanced Communications, Villanova University, Villanova, PA 19085 USA (e-mail: fauzia.ahmad@villanova.edu; yimin.zhang@villanova.edu; moeness.amin@villanova.edu).

Color versions of one or more of the figures in this paper are available online at http://ieeexplore.ieee.org.

Digital Object Identifier 10.1109/LGRS.2008.915742

beams. For a single point target located at $\mathbf{x_p} = (x_p, y_p, z_p)$, the output of the delay-and-sum beamformer, corresponding to the qth voxel at $\mathbf{x_q}$, is given by

$$z_q(t) = \sum_{m=1}^{M}\sum_{n=1}^{N} w_{tm} w_{rn} a(\mathbf{x_p}) e^{-\alpha(l_{mp,\text{wall}} + l_{np,\text{wall}})} \times s(t - \tau_{mn,p} + \tau_{mn,q}) \quad (1)$$

where $a(\mathbf{x_p})$ is the target reflectivity, w_{tm} and w_{rn} are the respective weights applied on transmit and receive, α is the attenuation constant of the wall, $l_{mp,\text{wall}}$ and $l_{np,\text{wall}}$ are the respective distances traveled inside the wall on transmit and receive, $\tau_{mn,p}$ is the propagation delay encountered by the signal as it propagates from the mth transmitter to the target and back to the nth receiver, and $\tau_{mn,q}$ is the aggregate of the focusing delays applied to the mth transmitter and the output of the nth receiver. The propagation and focusing delays are given by [5]

$$\tau_{mn,i} = \frac{(l_{mi,\text{air},1} + l_{ni,\text{air},1})}{c} + \frac{(l_{mi,\text{wall}} + l_{ni,\text{wall}})}{v} + \frac{(l_{mi,\text{air},2} + l_{ni,\text{air},2})}{c}$$
$$v = \frac{c}{\sqrt{\varepsilon}} \quad (2)$$

where $i = p$ for the target and $i = q$ for the qth voxel, c is the velocity of light in free space, and the subscripts "air, 1," "wall," "air, 2" denote, respectively, the distances before, through, and beyond the wall to $\mathbf{x_q}$ for $i = q$ and $\mathbf{x_p}$ for $i = p$. The complex amplitude image value $I(\mathbf{x_q})$ corresponding to the qth voxel is then obtained by applying a filter, matched to $s(t)$, to $z_q(t)$, and sampling the filtered data, as per the following:

$$I(\mathbf{x_q}) = z_q(t) * h(t)\big|_{t=0} = \sum_{m=1}^{M}\sum_{n=1}^{N} w_{tm} w_{rn} a(\mathbf{x_p}) e^{-\alpha(l_{mp,\text{wall}} + l_{np,\text{wall}})} \times s(t - \tau_{mn,p} + \tau_{mn,q}) * h(t)\big|_{t=0} \quad (3)$$

where $h(t) = s^*(-t)$ is the impulse response of the matched filter, the superscript * denotes complex conjugate, and "$*$" denotes convolution operator. The process, described in (1)–(3), is performed for all voxels in the region of interest to generate the image of the scene.

For a scene consisting of P point targets, the complex amplitude voxel value $I(\mathbf{x_q})$ can be obtained by superposition of the target reflections

$$I(\mathbf{x_q}) = \sum_{m=1}^{M}\sum_{n=1}^{N}\sum_{p=1}^{P} w_{tm} w_{rn} a(\mathbf{x_p}) e^{-\alpha(l_{mp,\text{wall}} + l_{np,\text{wall}})} \times s(t - \tau_{mn,p} + \tau_{mn,q}) * h(t)\big|_{t=0}. \quad (4)$$

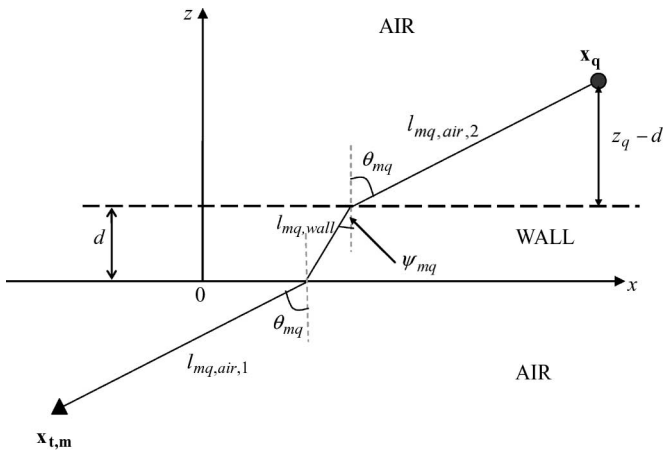

Fig. 2. Geometry on transmit of the equivalent 2-D problem when the transmitter and the voxel are at the same height.

The equivalent frequency-domain representation of the qth voxel value can be readily shown to be [8]

$$I(\mathbf{x_q}) = \sum_{m=1}^{M}\sum_{n=1}^{N}\sum_{p=1}^{P} w_{tm} w_{rn} a(\mathbf{x_p}) e^{-\alpha(l_{mp,\text{wall}} + l_{np,\text{wall}})} \times \frac{1}{2\pi}\int_{-\infty}^{\infty} |S(\omega)|^2 \exp\left(j\omega(t - \tau_{mn,p} + \tau_{mn,q})\right) d\omega\Big|_{t=0} \quad (5)$$

where $S(\omega)$ is the Fourier transform of the transmitted signal $s(t)$.

A. Computation of the Focusing Delays

The traveling distances inside and outside the wall, and, subsequently, the focusing delay, can be precisely computed, given the exact knowledge of the wall thickness and its dielectric constant. Consider first the traveling from the mth transmitter at $\mathbf{x_{tm}}$ to the qth voxel located at $\mathbf{x_q}$, as shown in Fig. 1. If both $\mathbf{x_q}$ and $\mathbf{x_{tm}}$ are at the same height, then the problem reduces to the equivalent 2-D problem, as shown in Fig. 2. The analytical expressions for the distances $l_{mq,\text{air},1}$, $l_{mq,\text{wall}}$, and $l_{mq,\text{air},2}$ for the 2-D problem were derived in [4] and [5] and are given by

$$l_{mq,\text{air},1} = \frac{z_{\text{off}}}{\cos(\theta_{mq})}$$
$$l_{mq,\text{wall}} = \frac{d}{\cos(\psi_{mq})}$$
$$l_{mq,\text{air},2} = \frac{(z_q - d)}{\cos(\theta_{mq})} \quad (6)$$

where θ_{mq} is the angle of incidence and ψ_{mq} is the angle of refraction, which can be computed by solving

$$(x_q - (x_{tm} + z_{\text{off}} \tan\theta_{mq}))^2 + z_q^2 = l_{mq,\text{wall}}^2 + l_{mq,\text{air},2}^2 - 2 l_{mq,\text{wall}} l_{mq,\text{air},2} \times \cos(\pi + \psi_{mq} - \theta_{mq})$$
$$\psi_{mq} = \sin^{-1}\left(\sin(\theta_{mq})/\sqrt{\varepsilon}\right). \quad (7)$$

Equations (6) and (7) represent a very specific case in which the array elements and the scene voxels lie in the same horizontal plane. The general case corresponds to $\mathbf{x_q}$ and $\mathbf{x_{tm}}$ assuming different heights. One approach for representing the general case forming the corresponding 3-D image behind walls simply builds on the aforementioned 2-D imaging equations. A rotation transform can be applied so that, in the new coordinate system, the mth transmitter and the qth voxel are at the same height, i.e.,

$$\begin{bmatrix} x'_{tm} \\ y'_{tm} \end{bmatrix} = \begin{bmatrix} \cos\beta & \sin\beta \\ -\sin\beta & \cos\beta \end{bmatrix} \begin{bmatrix} x_{tm} \\ y_{tm} \end{bmatrix}$$
$$\begin{bmatrix} x'_{q} \\ y'_{q} \end{bmatrix} = \begin{bmatrix} \cos\beta & \sin\beta \\ -\sin\beta & \cos\beta \end{bmatrix} \begin{bmatrix} x_{q} \\ y_{q} \end{bmatrix} \tag{8}$$

such that $y'_{tm} = y'_q$. This implies that

$$\tan\beta = \frac{y_{tm} - y_q}{x_{tm} - x_q}. \tag{9}$$

The earlier transformation preserves the angle of incidence and, as such, does not alter the traveling distance outside and inside the wall between the points $\mathbf{x_q}$ and $\mathbf{x_{tm}}$. Equations (6) and (7) can then be directly applied to compute the traveling distances with x_{tm} and x_q replaced by $x'_{tm} = \cos\beta x_{tm} + \sin\beta y_{tm}$ and $x'_q = \cos\beta x_q + \sin\beta y_q$, respectively.

The traveling distances, $l_{nq,\mathrm{air},1}$, $l_{nq,\mathrm{wall}}$, and $l_{nq,\mathrm{air},2}$, from $\mathbf{x_q}$ to the nth receiver at $\mathbf{x_{rn}}$ can be similarly computed and are given by (6)–(9) with $\mathbf{x_{tm}}$ and subscript m replaced by $\mathbf{x_{rn}}$ and subscript n, respectively.

III. Simulation Results

Computer simulations, implementing the frequency-domain representation of (5), were performed in MATLAB to verify the analysis of Section II. The simulation parameters are as follows. A stepped-frequency signal[1] of 2-GHz bandwidth centered at 2 GHz, with 201 steps of size 10 MHz, is used for imaging. The signal spectrum $S(\omega)$ is assumed to be constant over the bandwidth. A 33-by-33 element planar array with an interelement spacing of 7.5 cm on a square grid is used. The center of the grid is at $(x, y) = (0, 3)$ m. The center element acts as a transceiver, whereas all the other elements are used as receivers. Unit weights were applied to the transmit and receive elements. The wall through which the system is looking is a 9-cm-thick brick wall with $\varepsilon = 4.2$ and $\alpha = 54.3$ dB/m. For each of the 201 frequencies, the signal returns from a single point target at all 1089 receiver locations are computed as the complex amplitudes of the scaled and frequency-dependent phase-shifted versions of the transmitted complex exponentials. The returns due to multiple targets are obtained by adding the corresponding returns from each point target.

[1]A stepped-frequency approximation to (5), which uses a finite number K of monochromatic signals with equispaced frequencies ω_k covering the desired bandwidth $\omega_K - \omega_1$ is given by [8]

$$I(\mathbf{x_q}) = \frac{1}{2\pi} \sum_{\mathrm{k}=1}^{\mathrm{K}} \sum_{m=1}^{M} \sum_{n=1}^{N} \sum_{p=1}^{P} w_{tm} w_{rn} \left|S(\omega_k)\right|^2 a(\mathbf{x_p}) \times e^{-\alpha(l_{mp,\mathrm{wall}} + l_{np,\mathrm{wall}})} \exp\left(-j\omega_k(\tau_{mn,p} - \tau_{mn,q})\right).$$

This expression forms the basis of the stepped-frequency implementation used in the simulations.

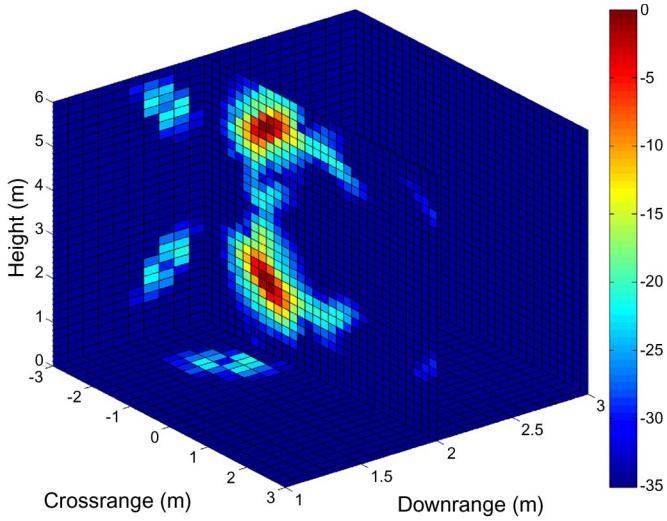

Fig. 3. 3-D image of two point targets with unit reflectivity, located at (−1.5, 1.5, 2) and (−1.5, 5, 2) m, respectively. The array standoff distance is 10 m.

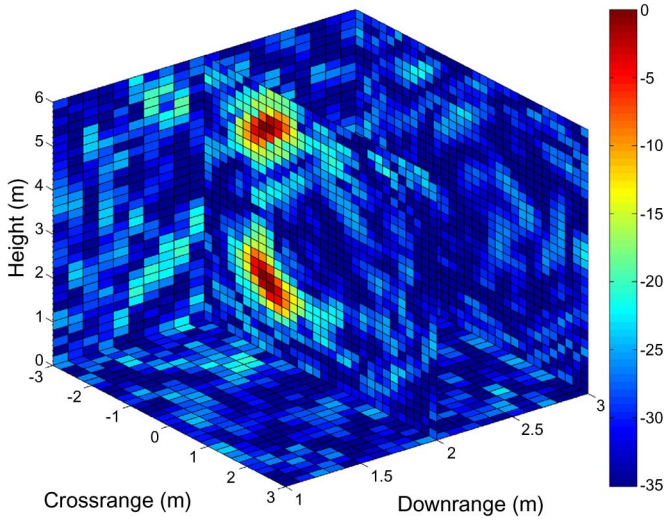

Fig. 4. 3-D image of the two point targets of Fig. 3 in the presence of complex Gaussian noise with an SNR of −20 dB.

Consider a scene consisting of two point targets, each of unit reflectivity, located at (−1.5, 1.5, 2) and (−1.5, 5, 2), the units being meters. Note that the targets are present at the same crossrange and downrange but are at different heights. The array is placed at a standoff distance of 10 m from the wall. Transformation (7) is applied to each voxel and array element prior to beamsteering. Fig. 3 shows the corresponding 3-D image of the scene. We observe that the beamformer has located both targets correctly. An image of the same scene in the presence of complex additive Gaussian noise with a signal-to-noise (SNR) ratio of −20 dB is shown in Fig. 4, which again shows the two targets at the correct locations.

Fig. 5 shows the 3-D image of a scene consisting of two extended targets of different lengths located at the same downrange, obtained with the array at a standoff distance of 3 m

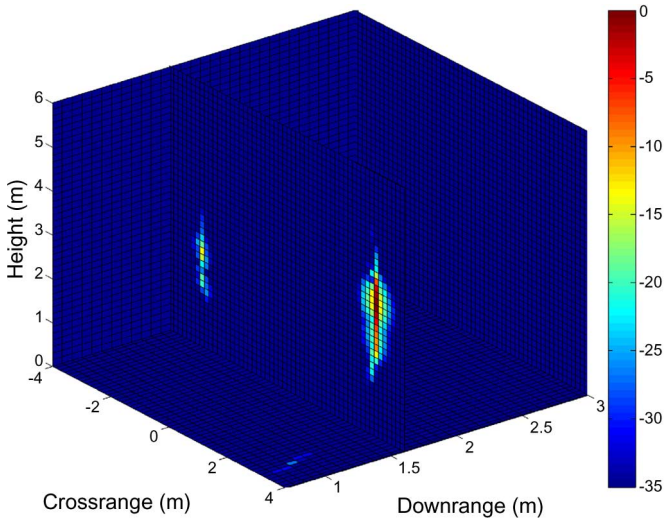

Fig. 5. 3-D image of two extended targets. Shorter target of height 0.52 m is located at (−3, 1.5, 1.6) m, and the taller target of height 1.42 m is located at (3, 2, 1.6) m. The array standoff distance is 3 m.

from the brick wall. The shorter target is located at a crossrange of −3 m and a downrange of 1.6 m. It extends vertically from 1.5 to 2.02 m, i.e., it is 0.52 m high and is assumed to have unit reflectivity across its extent. The taller target has a vertical span of 1.42 m and extends from 2 to 3.42 m, with a uniform reflectivity of three. It is located at a crossrange of 3 m and a downrange of 1.6 m. We can clearly see that the through-the-wall beamformer has not only localized the targets accurately but it is also possible to distinguish between targets of different heights. This capability is essential for through-the-wall applications where the distinction between animate objects like people and animals or between a person standing or sitting is of considerable interest.

IV. Conclusion

We have presented an approach for designing a 3-D through-the-wall beamformer for imaging through a single uniform wall. It is based on applying a transformation that brings the target and the transmitter/receiver to the same height, allowing the incorporation of time delays corresponding to 2-D beamforming through walls. The effects of propagation through the wall material have been incorporated in the design, allowing effective and reliable imaging of scenes behind walls. Supporting simulation results have been provided, which demonstrate the ability of the beamformer to accurately localize and distinguish between objects of different heights.

References

[1] Y. Yunqiang and A. E. Fathy, "See-through-wall imaging using ultra wideband short-pulse radar system," in *Proc. IEEE AP-S Int. Symp.—Special Session Through-Wall Imaging Sensing*, Jul. 2005, vol. 3B, pp. 334–337.

[2] S. E. Borek, "An overview of through the wall surveillance for homeland security," in *Proc. 34th Appl. Imagery and Pattern Recog. Workshop*, Oct. 2005, pp. 42–47.

[3] L.-P. Song, C. Yu, and Q. H. Liu, "Through-wall imaging (TWI) by radar: 2-D tomographic results and analyses," *IEEE Trans. Geosci. Remote Sens.*, vol. 43, no. 12, pp. 2793–2798, Dec. 2005.

[4] F. Ahmad, M. G. Amin, and S. A. Kassam, "Synthetic aperture beamformer for imaging through a dielectric wall," *IEEE Trans. Aerosp. Electron. Syst.*, vol. 41, no. 1, pp. 271–283, Jan. 2005.

[5] G. Wang and M. G. Amin, "Imaging through unknown walls using different standoff distances," *IEEE Trans. Signal Process.*, vol. 54, no. 10, pp. 4015–4025, Oct. 2006.

[6] F. Ahmad, M. G. Amin, and G. Mandapati, "Autofocusing of through-the-wall radar imagery under unknown wall characteristics," *IEEE Trans. Image Process.*, vol. 16, no. 7, pp. 1785–1795, Jul. 2007.

[7] D. H. Johnson and D. E. Dudgeon, *Array Signal Processing: Concepts and Techniques*. Englewood Cliffs, NJ: Prentice-Hall, 1993, ch. 4, pp. 111–113.

[8] F. Ahmad, G. J. Frazer, S. A. Kassam, and M. G. Amin, "Design and implementation of near-field wideband synthetic aperture beamformers," *IEEE Trans. Aerosp. Electron. Syst.*, vol. 40, no. 1, pp. 206–220, Jan. 2004.